Baoqing Zhang
Department of Mechanical and Industrial Engineering, University of Iowa, Iowa City, IA 52242; College of Mechanical and Electrical Engineering, Changchun University of Science and Technology, 7089 Weixing Road, Changchun 130022, China; Changchun Institute of Optics, Fine Mechanics and Physics, Chinese Academy of Sciences, 3888 Dongnanhuda Road, Changchun 130033, China

Qinghua Wang
Department of Mechanical and Industrial Engineering, University of Iowa, Iowa City, IA 52242

Ninggang Shen
Department of Mechanical and Industrial Engineering, University of Iowa, Iowa City, IA 52242

Hongtao Ding[1]
Department of Mechanical and Industrial Engineering, University of Iowa, Iowa City, IA 52242
e-mail: hongtao-ding@uiowa.edu

Experimental Investigation and Numerical Analysis of Mechanical Ruling for an Aluminum-Coated Diffraction Grating

The mechanical ruling process using a diamond tool is an important method for fabrication of low-density diffraction gratings. In mechanical ruling, a deposited film of aluminum or gold is mechanically burnished by the diamond tool to form equally spaced and high-quality grooves. The goal of this work is to evaluate the effects of Al film properties and ruling tool loading conditions on the resultant groove formation. The microstructure of the Al film is first studied using scanning electron microscope (SEM) and X-ray diffraction (XRD). The mechanical properties of the Al film are measured by nano-indentation and scratch tests. Mechanical ruling experiments are then carried out on a 10.5 μm thick Al film under various ruling loads ranging from 20 to 105 g. The groove geometry is investigated, and the tool wear of the diamond tool is inspected after the mechanical ruling tests. Finally, a three-dimensional (3D) thermomechanical-coupled finite-element (FE) model is developed to predict the deformation and temperature fields for the micron-scale groove formation by incorporating the Al film properties and a strain-gradient plasticity for modeling the size effect. Multiruling pass simulations are performed to analyze the groove formation under different loading conditions. Through comparison of simulation results with experimental measurement, this model is demonstrated as a useful numerical tool for modeling the mechanical ruling process using a diamond tool. [DOI: 10.1115/1.4034282]

Keywords: mechanical ruling, diffraction grating, aluminum film, diamond tool, finite-element model, size effect

1 Introduction

Diffraction gratings refer to reflecting or transparent optical components with a periodic structure, which splits and diffracts light into several beams traveling in multiple directions. They have been used in numerous optical instruments, such as laser scanners, monochromators, optical pulse compressing devices, spectrometers, and wavelength division multiplexing devices. Main fabrication methods of diffraction gratings include mechanical ruling, ion beam etching, holography, and replication. Among the various fabrication methods, mechanical ruling is usually applied to make a low-density diffraction grating and is currently the only valid option for fabrication of infrared gratings and echelle gratings [1].

Mechanically ruled master gratings are fabricated by mechanically burnishing of an evaporated thin film of gold (Au) or aluminum (Al) using a precision diamond tool. During the mechanical ruling process, little materials are removed from the process under micron scale. Multiple fine, parallel, equally spaced grooves are formed on the film as a result of elastoplastic deformation. The groove density for mechanically ruled diffraction gratings ranges up to 2000 grooves/mm, i.e., minimum of 0.5 nm [1]. The triangular groove profile must be accurately controlled across the entire surface of the grating. The process condition, in particular, the ruling tool wear, has to be constantly monitored and compensated to ensure a tight control of the ruled groove profile. These high-standard specifics required by the gratings demand a high degree of precision. As a result, only a few number of facilities in the world are able to mechanically rule the master gratings.

Numerous efforts have been devoted in the last century for the development of the grating ruling engine since the invention of the world's first diffraction grating [2–4]. In 1910 s, Wood [5] discovered the art of blazing and produced low ruling density (40–80 grooves/mm) infrared gratings. Later, Davies and Stiff [6] conducted grating ruling tests with different ruling densities and obtained the relation between the diffraction efficiency and groove density. Verrill [7,8] discussed systematic alignment of a diffraction ruling tool and proposed that ruling tool wear could be eliminated by examining a trial ruling. In 1980 s, Harada et al. [9] studied the formation of groove profile and found the effectiveness of the groove space variation technology for reducing aberrations in concave grating monochromators. Recently, Zhang et al. [10,11] found that the attributes of deposited Al film played an important role in the ruling process, and the groove formation was highly sensitive to the film preparation as well as the process condition.

The reflective Al film is often prepared by physical vapor deposition (PVD) method on the glass substrate. In mechanical ruling, an Al film with a 10–15 μm thickness is often required to guarantee a satisfying groove depth. However, most of the past research efforts have been focused on PVD coatings with a thickness less than 5 μm using various characterization techniques [12–17]. In addition, the mechanical properties of the Al film should also be quantitatively determined for an accurate process model.

[1]Corresponding author.

Manuscript received March 8, 2016; final manuscript received July 5, 2016; published online August 24, 2016. Assoc. Editor: Donggang Yao.

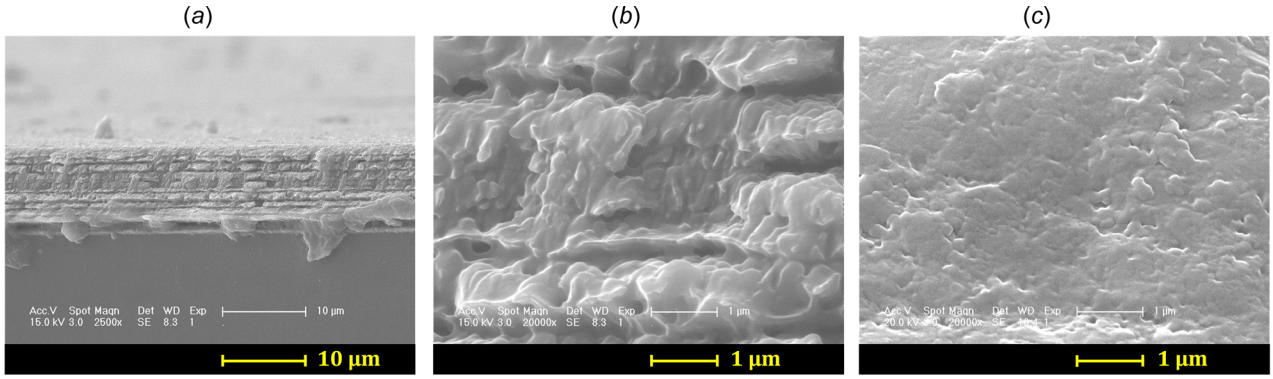

Fig. 1 SEM micrographs of the Al film: (*a*) side view, (*b*) zoom-in of the side view, and (*c*) top surface

Nano-indentation test is often implemented for evaluating the hardness and Young's modulus of different PVD coatings [18,19]. The material response and formability of the Al film with a deformation in micron scale under the mechanical ruling condition have not been well understood in the previous literature.

A few numerical analyses have been conducted to simulate the groove formation during mechanical ruling. Sokolova [20] developed a geometric theory for a spherical mechanically ruled concave diffraction grating and simulated the curved grooves with this technology. Zhang et al. [10,11] developed a three-dimensional (3D) finite-element (FE) model to simulate the mechanical ruling process with multiple ruling tool geometries and determined an optimal set of process parameters. However, the critical film quality and size effect during the grating ruling process were not considered in their work. Due to the small ruling load (less than 100 g force), the grooves are formed with a depth of 3–5 μm, and hence a significant size effect exists during the elastoplastic deformation under this micron scale.

To effectively design and control the mechanical ruling process for various diffraction gratings, it is necessary to investigate the effects of film preparation and tool loadings for this elastoplastic deformation process and is desirable to have an analytical solution for predicting the groove geometry. The research objectives of this study are first to evaluate the Al film preparation technique in terms of surface integrity and mechanical properties, and then to quantify the effect of ruling tool loading condition on the resultant groove formation using experimental and numerical analyses. In this work, the preparation technique of the Al film is thoroughly studied in terms of film surface morphology, nanohardness, and elastic modulus. An experimental analysis is then conducted to investigate the groove geometry and effect of ruling loads. Finally, a 3D thermomechanical-coupled FE model is developed to simulate the mechanical ruling process for predicting the deformation and temperature fields.

2 Film Preparation and Characterization

2.1 Film Preparation. In this study, pure Al was deposited on the K-9 glass substrate using the PVD method of vacuum evaporation. During the PVD process, the Cr evaporation source was first heated to deposit the transition layer. Then, multiple Al evaporation sources were activated to deposit multiple layers of Al film on the glass substrate. In this research work, a 10.5 μm thick Al film was deposited onto the K-9 glass substrate using six Al evaporation sources. The film surface morphology was investigated by scanning electron microscope (SEM). Figure 1(*a*) shows the side view of the Al film composed of six layers from the six evaporation sources. A zoom-in side view as can be seen in Fig. 1(*b*) shows diffused tiny fibrous/columnar crystals illustrating grain growth on the film side with the high substrate temperature. Figure 1(*c*) shows the SEM micrograph of the top film surface of the Al film. A smooth surface was observed for the film after a long deposition time with six evaporation sources.

The surface roughness of the Al film top surface was measured using a white-light interferometer. The surface roughness R_a of the prepared Al film is about 0.135 μm. In order to verify the crystallization of the deposited Al film, X-ray diffraction (XRD) was performed using a Cu-K_α radiation with a wavelength of 0.15418 nm.

Figure 2 shows the measured XRD pattern of the Al film. One significant high peak of (111) plane and four other tiny peaks can be observed in Fig. 2. The XRD spectra showed that the diffraction angles of (111) plane were very close to the Bragg's angle of 38.43 deg for pure Al, which indicated that the coating was almost strain-free. These findings indicated that the all the coatings had a preferred orientation of ⟨111⟩. It implied that this preferred orientation resulted in the most densely populated atomic planes parallel to the substrate [21].

2.2 Nano-Indentation Tests. Young's modulus and hardness of the Al film were examined with nano-indentation tests. The nano-indentation tests were conducted with a commercial nano-indenter TriboIndenter (Hysitron Inc., Eden Prairie, MN) equipped with a Berkovick indenter using a load range of 10 mN and large indentation depth. After the calibration tests, the Al film was indented ten times with an incremental indentation depth of 0.5 μm, i.e., 0.5 μm depth after the first indentation and 5 μm depth after the 10th indentation. For each indentation, both of the loading time and unloading time were set 10 s. The elastoplastic properties of each indent were measured six times in order to minimize the effect of the uneven mass of the Al film. Figure 3 shows the load–displacement curves for all the ten indentations. The load–displacement data was directly obtained by the nano-indenter, which could minimize the influence of different calculation methods and the indenter tip passivation. For all the tests, the

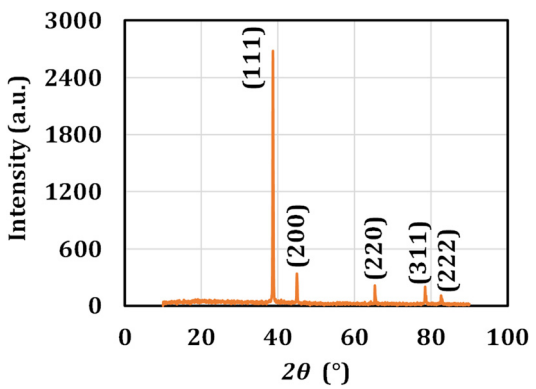

Fig. 2 XRD patterns of the fabricated Al film

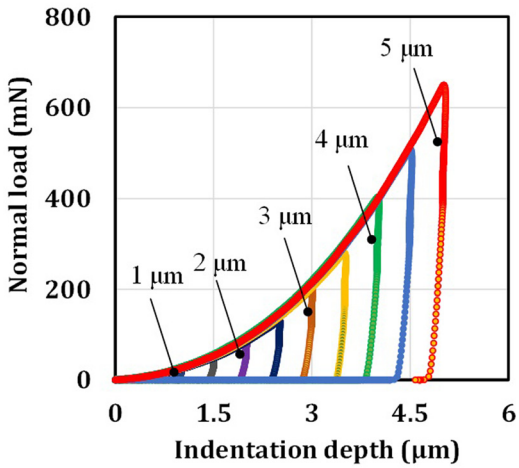

Fig. 3 Load–indentation response curve for various indentation depths

loading curves overlapped with each other very well, and the unloading curves were all parallel. These findings indicated the stability of the nano-indentation test for the Al film.

From the load–displacement curves, Young's modulus, E, and hardness, H, of the film were calculated based on the maximum indentation depth, h_m, and residual indentation depth, h_f. The average Young's modulus and hardness were 87.7 GPa and 631.7 MPa, respectively. Figure 4 shows the measured data of Young's modulus and hardness with varying indentation depths. Due to a strong size effect in this length scale, both E and H were decreased within an indentation depth of 2 μm. Large fluctuation can be observed for the test results at smaller indentation depths indicating the inhomogeneity of the Al film. The fluctuation gradually attenuated with the increase of the indentation depth.

The springback during the nano-indentation test was also evaluated. Based on the load–displacement curves in all the tests, the largest springback values h_r can be determined by the following equation:

$$h_r = h_m - h_f \tag{1}$$

where h_m is the maximum indentation depth, and h_f is the residual indentation depth. Figure 5 shows the relative springback in all the nano-indentation tests. The relative springback at the indent bottom decreased from 8% to 5.5%, as the indentation depth increased from 0.5 to 5 μm. The combined effects of the soft film and hard substrate were not noticeable. Thus, the springback on the residual indent surface would gradually decrease as the indentation depth increases. These characteristics will be critical to understand the springback performance of the prepared Al film during the grating ruling experiments.

Scratch tests were conducted to measure the friction coefficient between the diamond indenter and the Al film surface using the nano-indentation device. In order to accurately measure the friction coefficient, the Al film was scratched four times with varying maximum normal loads. The normal load was applied starting from the fifth second, and the probe started to penetrate into the Al film. After the probe reached the maximum penetration depth at tenth second, the normal force remained as constant for 20 s. Then, it started to unload for 5 s, while the probe was gradually lifted and detached with Al film within 5 s. The friction coefficient can be calculated using equation $f = L/N$ (L is the normal force, and N is the lateral force). Friction coefficient values from four stable scratch tests were averaged to minimize the experimental error. The average friction coefficient at stable condition was determined to be 0.51 from these scratch tests.

3 Mechanical Ruling Experiments

The mechanical ruling experiments were conducted for the Al-coated specimens on a grating ruling engine designed and manufactured by Changchun Institute of Optics, Fine Mechanics and Physics, Chinese Academy of Sciences, Changchun, China. The experimental process and tool path are schematically illustrated in Fig. 6(*a*). The grating was ruled on the Al film using a wedge-shaped single crystalline diamond ruling tool as depicted in Fig. 6(*c*). The diamond tool was joined onto the carbide tool base with a length of 20 mm and a bottom area of 2.35 mm^2. The tool material had a high thermal conductivity of 1.5 kW/m K at room temperature. A grating density of 79 grooves/mm was desired for these experiments. A constant ruling speed of 60 mm/s was applied for the diamond tool in all these experiments. The tool was tilted by 4 deg from the horizontal plane in the ruling direction. Multiple experiments with the vertical ruling loads varying from 20 g to 115 g were investigated in this study. Figure 6(*c*) shows a good sample diffraction grating fabricated after the experiment.

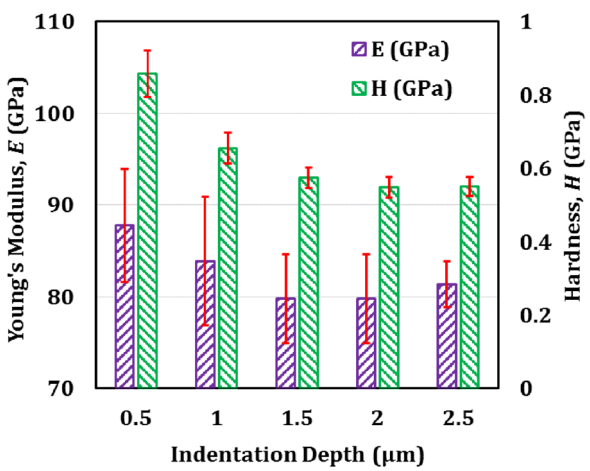

Fig. 4 Nano-indentation results

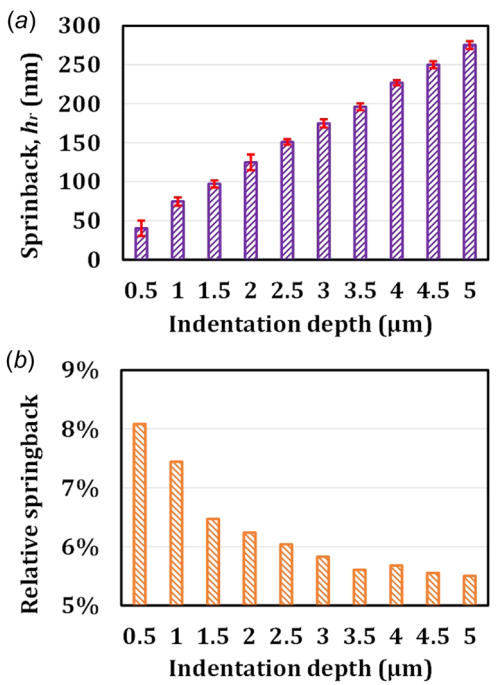

Fig. 5 Springback measurement from nano-indentation tests: (*a*) springback and (*b*) relative springback

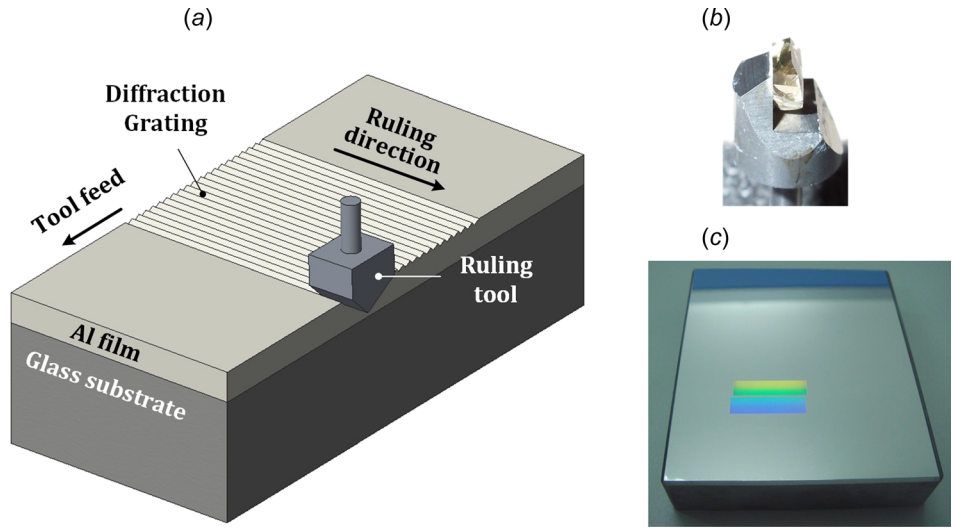

Fig. 6 Ruling tool and workpiece: (*a*) schematic of the mechanical ruling process, (*b*) diamond tool, and (*c*) a fabricated diffraction grating

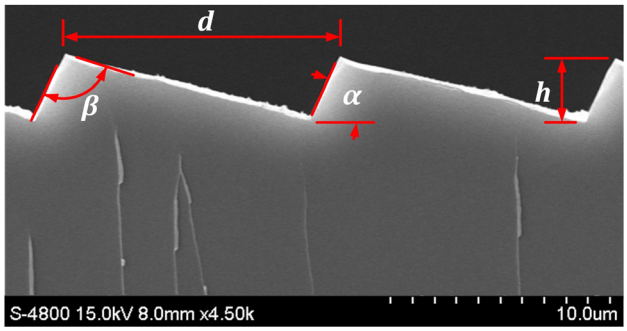

Fig. 7 SEM micrograph of fabricated grating grooves with the designated groove form variables labeled

Microscopic examination of the grating groove form was performed using both optical microscope and SEM. Figure 7 shows a micrograph of fabricated grating grooves with the designated groove form parameters. The form parameters investigated by this study are listed in Table 1. The shorter side surface is the blazing surface, i.e., the working plane of the grating. Based on the theoretical calculation, this type of groove geometry will typically result in a higher diffraction efficiency.

Figure 8 shows the optical micrograph of the beginning, middle and end of multiple grating grooves. A uniform spacing was kept along the ruling direction among successive grooves. Figure 9(*a*) further examines the 3D height profile of the grating grooves from an optical surface profiler. In order to investigate the form integrity, a typical 2D height profile of the grooves was extracted as shown in Fig. 9(*b*). The cross-sectional areas of the grating structure above (S_i) and below (A_i) the original film surface were calculated based on the 2D height profile. The equivalent cross-sectional areas for above and below the original film surface indicated that a sound grating structure was formed with little material removed from the film from the mechanical ruling process.

The grating groove profiles produced by various ruling loads are shown in Fig. 10. With insufficient ruling loads of 20–40 g, the groove depth was too shallow to form the proper grooves as can be seen in Figs. 10(*a*) and 10(*b*). The sharp groove top angle was not formed from these light loads and a flat area remained between two neighbor grooves. As the ruling load increased to 70–80 g, grooves with a high-quality form accuracy were formed as shown in Figs. 10(*c*) and 10(*d*). As the ruling load was increased to above 100 g as shown in Figs. 10(*e*) and 10(*f*), incorrect grooves were formed with the tip of grooves severely distorted by the following ruling passes. These findings indicate that 70–80 g ruling loads were optimum for the 10.5 μm thick Al film, and the form accuracy of the mechanical ruling process is highly dependent on the ruling load and material property.

To fabricate a large diffraction grating, e.g., 410×614 mm^2 in area, the ruling tool needs to travel for about 19.89 km, which is a long and painstaking process. After traveling such a long distance, severe tool wear can be observed on the ruling tool as shown in Fig. 11. Severe abrasive tool wear was observed along the cutting edge on the primary rake face and on the edge next to the back relief surface. These wear occurred along the material flow direction during the ruling process. Therefore, the tool wear condition needs to be constantly monitored and compensated to maintain the groove form accuracy. An accurate process model can be developed to predict the material flow and tool surface pressure to evaluate the tool wear rate during the ruling process. These studies will help process planning of the ruling experiment over a large area and determine the time to readjust the diamond tool during the process.

4 Process Modeling

To better understand mechanical ruling process of diffraction gratings, a 3D thermomechanical-coupled FE model was developed in DEFORM® to predict the deformation and temperature fields. The material constitutive model of strain-gradient plasticity was used in this FE analysis to study the size effect of the micron-scale groove-forming process.

4.1 Material Constitutive Model. The significant size effect during the mechanical ruling process was modeled using a strain

Table 1 Form parameters of the diffraction grating

Groove density, n (grooves/mm)	Groove spacing, d (μm)	Blaze angle, α (deg)	Groove top angle, β (deg)	Groove depth, h (μm)
79	12.66	64.5	85–90	2–6

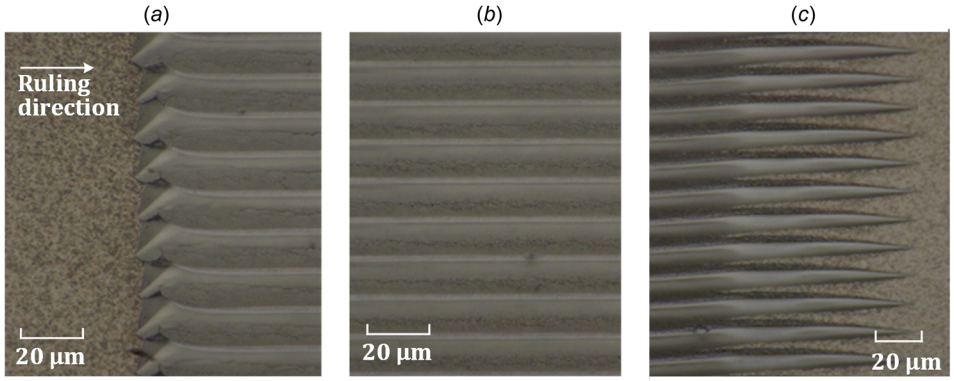

Fig. 8 Optical microscopy of grating grooves: (*a*) beginning, (*b*) middle, and (*c*) end of grating grooves

gradient-based constitutive model. This constitutive model is briefly described in this part, and more details can be found in Refs. [22–26]. In this model, a length scale can be developed using the coefficients of spatial gradients of strain components and it can be a useful tool for modeling the size effect during mechanical ruling. The model is based on a modified Johnson–Cook constitutive equation which can be explicitly expressed in the following equation:

$$\sigma=(A+B\varepsilon^n)\left(1+C\ln\frac{\dot{\varepsilon}}{\dot{\varepsilon}_o}\right)\left(1-\left(\frac{T-T_{\text{ref}}}{T_m-T_{\text{ref}}}\right)^m\right)\left(1+\left(\frac{18\alpha^2bG^2}{L\left((A+B\varepsilon^n)\left(1+c\ln\frac{\dot{\varepsilon}}{\dot{\varepsilon}_o}\right)\left(1-\left(\frac{T-T_{\text{ref}}}{T_m-T_{\text{ref}}}\right)^m\right)\right)^2}\right)^{\mu}\right)^{1/2} \quad (2)$$

where ε, $\dot{\varepsilon}$, and $\dot{\varepsilon}_o$ are the effective strain, effective strain rate, and reference strain rate, respectively; T_m and T_{ref} are the material melting temperature and process reference temperature, respectively; A, B, C, m, and n are the material constants in Johnson–Cook model; α and μ are the empirical coefficients; b is the Burgers vector; G is the shear modulus; and L is the length parameter. L used in this study was chosen to be the ruling depth for the corresponding mechanical ruling test. For example, L was 3 μm for the ruling load of 70 g. The model parameters are listed in Table 2 for pure Al. The values of α and μ were adopted from Ref. [22]. The mechanical and physical properties of pure Al and the tool material of diamond used in the simulation are listed in Table 3, while the Young's modulus was set to 87.7 GPa from the nano-indentation tests.

4.2 Finite-Element Model. The mechanical ruling process of diffraction grating was modeled using a commercial 3D forming process software DEFORM®. Figure 12 shows the 3D FE model setups for the tool and Al-coated workpiece. The ruling diamond tool was modeled using PTC Creo® with the design parameters mentioned and imported into the simulation software as a rigid body. The workpiece simulation domain was set as a rectangle with 0.15×0.2 mm^2 in x–y dimensions. The 10.5 μm thick Al film was modeled as an elastoplastic body with the strain-gradient constitutive model. A 0.1 mm thick glass substrate was modeled below the Al film as a heat sink.

A coupled thermomechanical analysis was carried out to study the deformation and heat transfer in mechanical ruling. Constant temperature boundary condition of 25 °C was set at the top of the ruling tool and bottom of the glass substrate. A thermal conductance was given as 5000 W/m^2 K at all the contact interfaces to maintain the temperature continuity during the simulation [24,29,30]. The ruling tool was tilted by 4 deg in the model and given a speed of 60 mm/s in the y-direction. The total ruling displacement was set to be 0.2 mm per stroke with a step increment of 0.1 μm/step. Different pressure values were applied on the top of the ruling tool to model the various ruling loads applied on the Al film. The friction coefficient was set to 0.51, which was obtained from the scratch tests with the nano-indenter.

Tetrahedral elements were used to mesh the ruling tool and the Al film. For the Al film, 174,706 elements were used with a minimum element size of 1.2 μm. For the ruling tool, 25,723 elements were used with a minimum element size of 1.4 μm. Mesh window

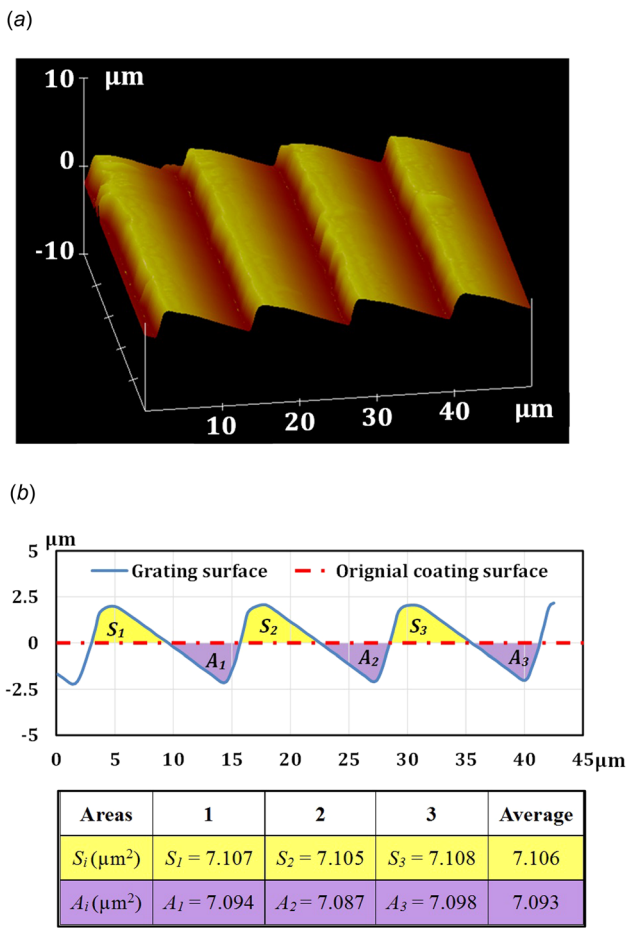

Areas	1	2	3	Average
S_i (μm^2)	S_1 = 7.107	S_2 = 7.105	S_3 = 7.108	7.106
A_i (μm^2)	A_1 = 7.094	A_2 = 7.087	A_3 = 7.098	7.093

Fig. 9 Grating grooves: (*a*) 3D profile of grating grooves and (*b*) cross section area comparison of the grating grooves

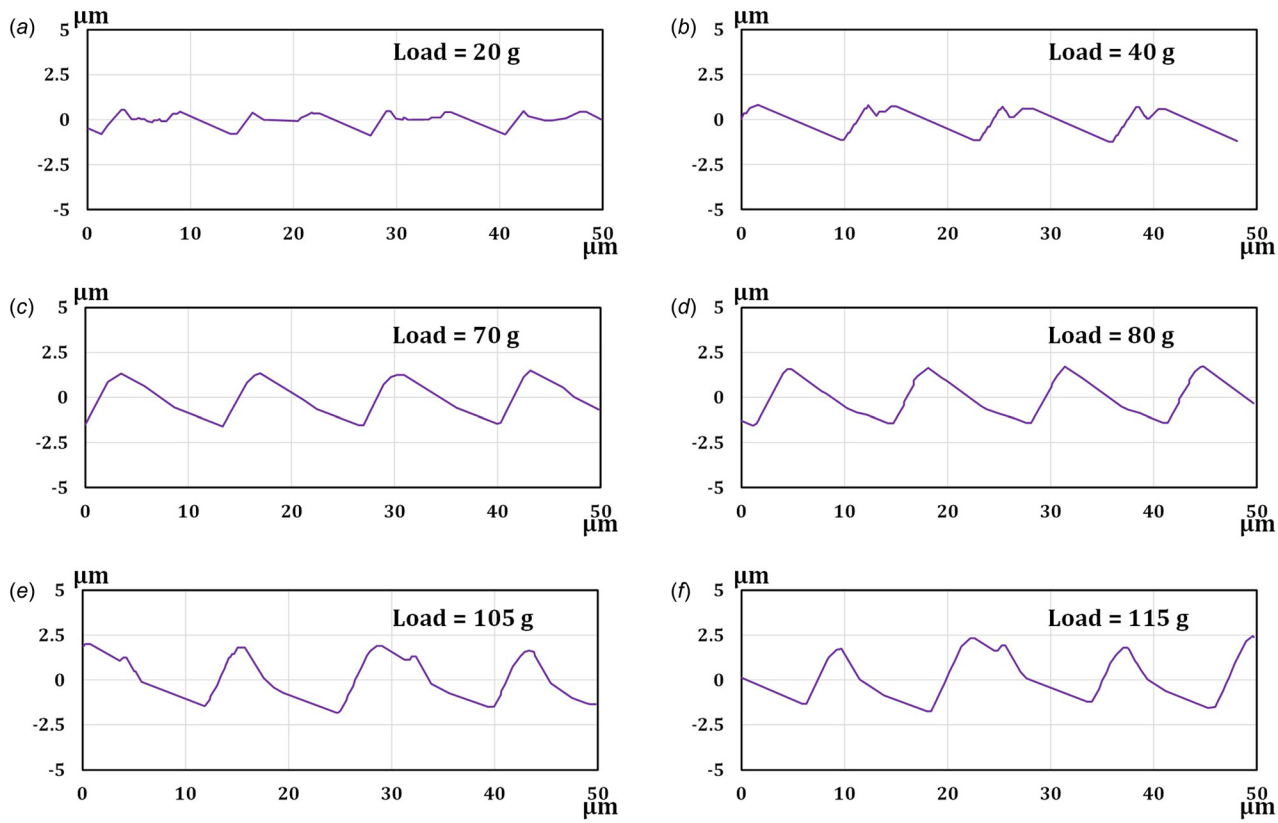

Fig. 10 Groove profiles subjected to various ruling loads: (*a*) 20 g, (*b*) 40 g, (*c*) 70 g, (*d*) 80 g, (*e*) 105 g, and (*f*) 115 g

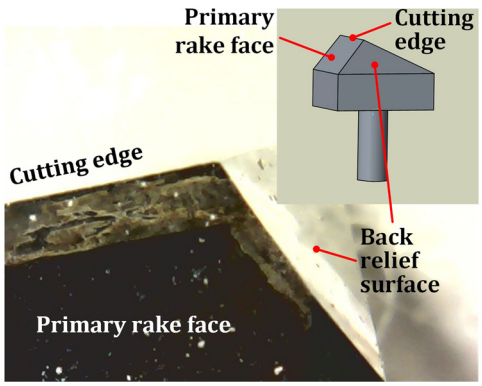

Fig. 11 Tool wear after mechanical ruling of an area of 410 × 614 mm²

and adaptive remeshing with a relative inference ratio of 0.7 were applied to ensure a good meshing quality during the simulations. Target volume control was set active in meshing and FE simulation in order to maintain the volume of the Al film unchanged during the mechanical ruling simulations [31,32]. Multiple ruling strokes were simulated with the 3D-coupled thermomechanical model. As the tool contacted the workpiece during the stroke, a fine mesh was generated by the adaptive remeshing algorithm within the defined domain. As the previous stroke simulation completed, the simulation results would be then carried over to the next stroke simulation.

5 Simulation Results

5.1 Multipass Ruling Simulation. Figure 13 shows the groove formation of three-pass simulation and their effective strain distributions. A significant increase in strain was simulated in the third pass compared with that of the first pass as shown in Figs. 13(*a*) and 13(*b*). This increase from 1.5 to 3 was because of the accumulation of plastic deformation between passes. The third pass was simulated based on the deformed material resulted from the previous two passes. Further simulation of more passes was considered unnecessary because insignificant difference was observed in the strain distribution from the second and third passes. In Fig. 13(*c*), it can be observed that from the first pass, the groove top angle was not completely formed. During the second pass, the sharp groove top angle was formed due to the superposition and interference from the two grooves, i.e., the material below the blaze surface of the second groove was pushed toward the nonblaze surface of the first groove. As a result, a proper groove top angle was formed between the first and second groove as shown in Fig. 13(*d*). As can be seen from Fig. 13(*e*), with the ruling load of 70 g, three grooves have been fabricated completely and properly with a similar groove geometry.

Figure 14 shows the simulated equivalent flow stresses, strain rates, and temperature for the first and third pass under a ruling load of 70 g. For the flow stress, it can be found that the stress for the third pass was slightly higher as shown in Figs. 14(*a*) and 14(*d*), which is attributed to work hardening during the mechanical ruling process. For the third pass, the strained material required a higher flow stress on the order of 735 MPa to deform.

Table 2 Johnson–Cook constitutive plasticity model parameters for pure aluminum [22,23,27]

Material	*A* (MPa)	*B* (MPa)	*N*	*C*	*m*	*G* (GPa)	*b* (nm)	α	μ
Aluminum	148.4	345.5	0.183	0.001	0.859	26	0.286	0.5	0.38

Table 3 Mechanical and physical properties of pure Al and diamond tool [27,28]

Properties	Al	Diamond
Elastic modulus (GPa)	87.7	850
Poisson's ratio	0.3	0.1
Specific heat (J/kg °C)	920	471.5
Thermal conductivity (W/m K)	237	1500
Thermal expansion (μm/m °C)	23.1	3
Density (g/cm^3)	2.7	3.5

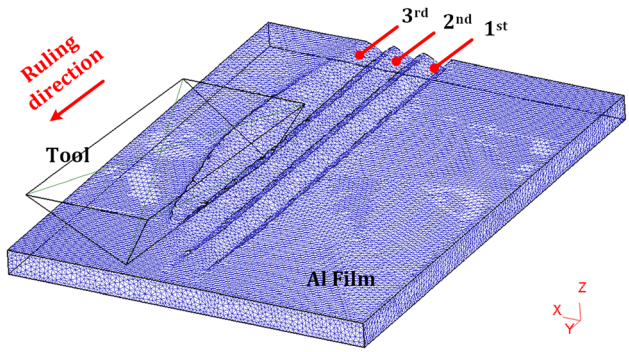

Fig. 12 Finite-element model configuration (with the glass substrate hidden from the view)

The strain rate of 2500 s^{-1} for the third pass was found slightly higher than the first pass as can be seen in Figs. 14(*b*) and 14(*e*). For the simulated temperature field, it was found that the maximum temperature occurred in the deformation zone during mechanical ruling, but the temperature increase was quite small. This is resulted from the limited heat generation due to plastic deformation and rapid heat dissipation due to the high thermal conductivity of the ruling tool and film materials. Therefore, the temperature of Al film can be assumed as the initial room temperature before each pass. These simulation results showed that further simulation of more passes was unnecessary since insignificant difference was observed in simulated fields from the second and third passes.

5.2 Groove Form Versus Ruling Load. To evaluate the FE model accuracy with the strain-gradient plasticity, four mechanical ruling conditions were simulated with various ruling loads of 20–105 g. The grooves corresponding to different ruling loads were simulated as shown in Fig. 15, and compared with the experimental results of groove profiles. It was found that the simulated groove forms matched well with the experimental measurements for all these loading conditions. The simulation results accurately captured the groove geometry features formed during the mechanical ruling experiments and indicated that an optimal load existed for the mechanical ruling process. For low ruling loads of 20 g and 40 g as shown in Figs. 15(*a*) and 15(*b*), the model accurately predicted a groove formation with an insufficient groove depth and tiny bumps and valleys between two adjacent grooves. These features predicted by the simulations were easily observed from the experimental results. The model predicted that good-quality grooves were formed free of defects under a ruling load of 70 g as can be seen in Fig. 15(*c*), which matched well the experimental results. Smooth groove top angles and blaze angles were found to be completely formulated as shown in both the experimental and simulation results. However, as the ruling load was increased to as large as 105 g, the model accurately predicted that the previous

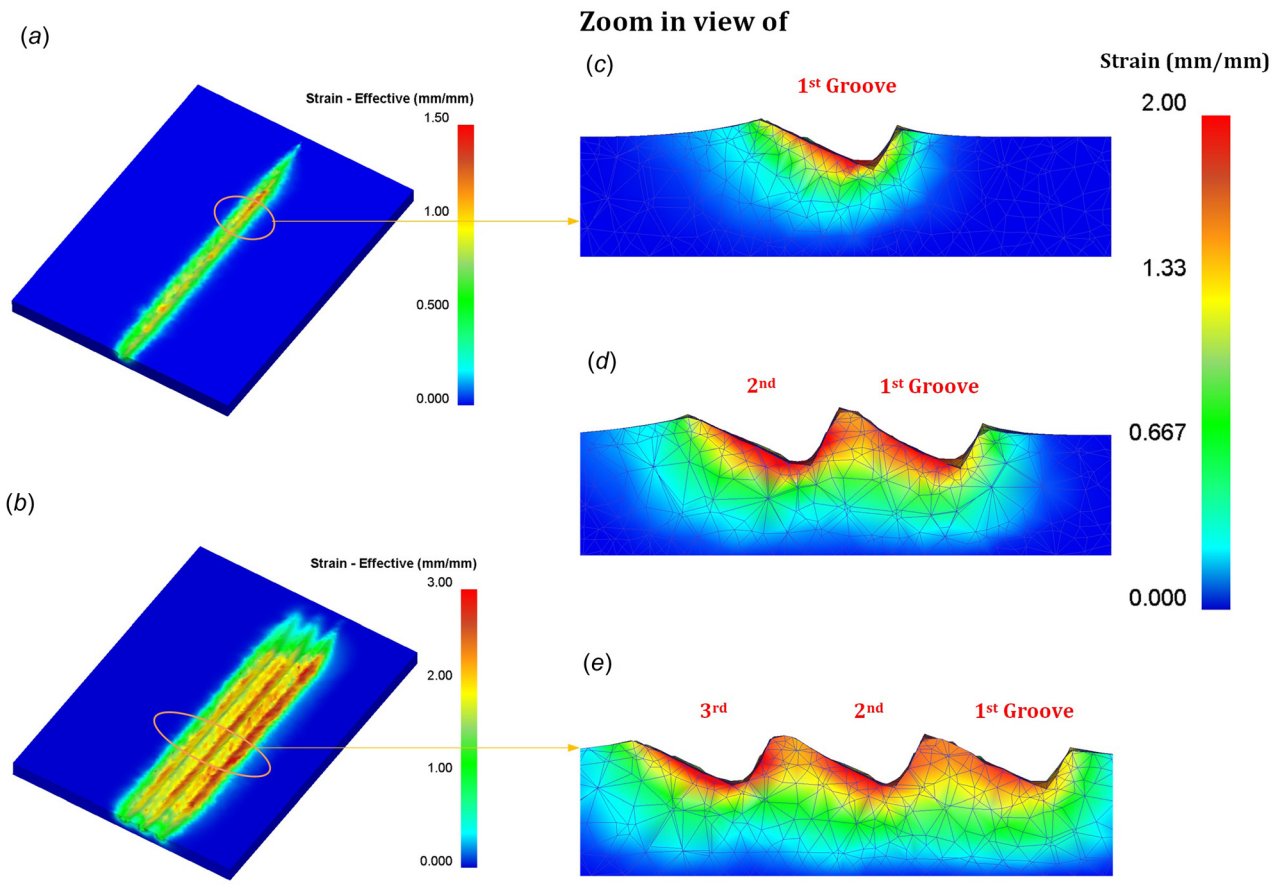

Fig. 13 Three-dimensional groove formation and strain distribution for different ruling passes of ruling load 70 g: (*a*) first pass, (*b*) third pass, (*c*) first pass, (*d*) second pass, and (*e*) third pass

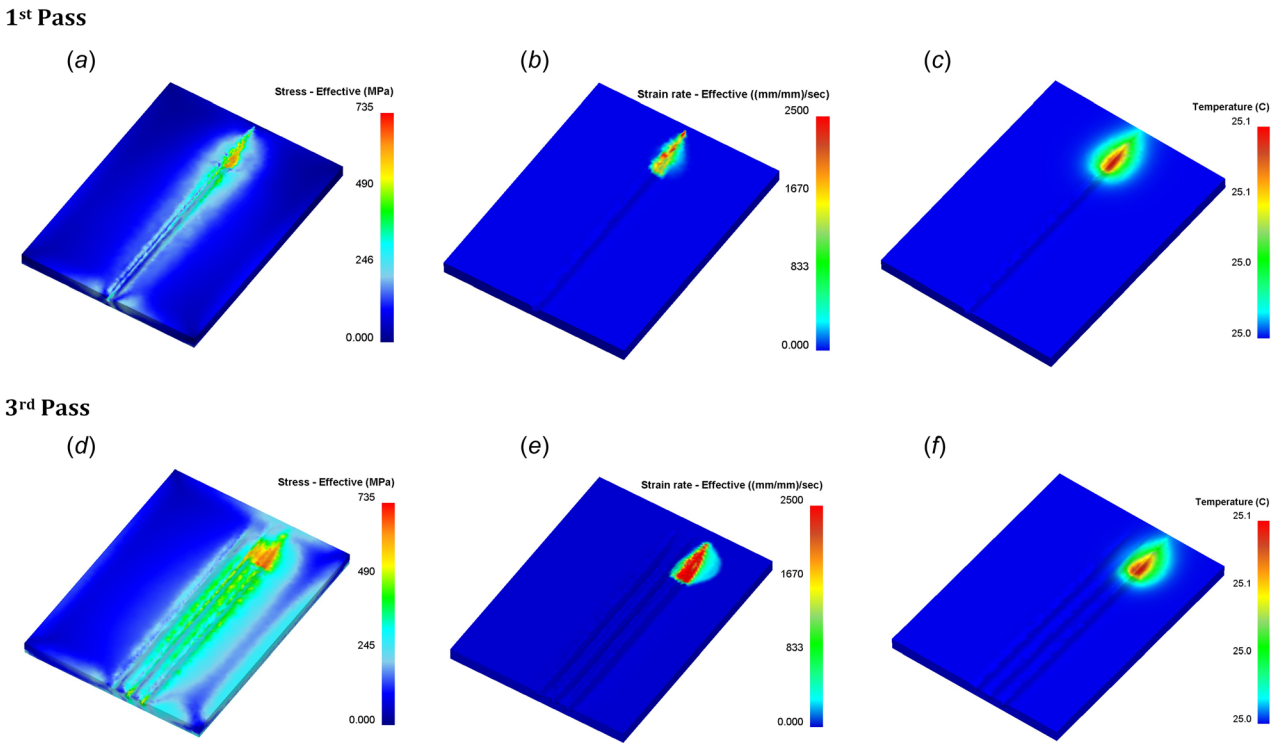

Fig. 14 Simulated flow stress, strain rate, and temperature under a ruling load of 70 g. First pass: (*a*) Von Mises stress, (*b*) effective strain rate, and (*c*) temperature. Third pass: (*d*) Von Mises stress, (*e*) effective strain rate, and (*f*) temperature.

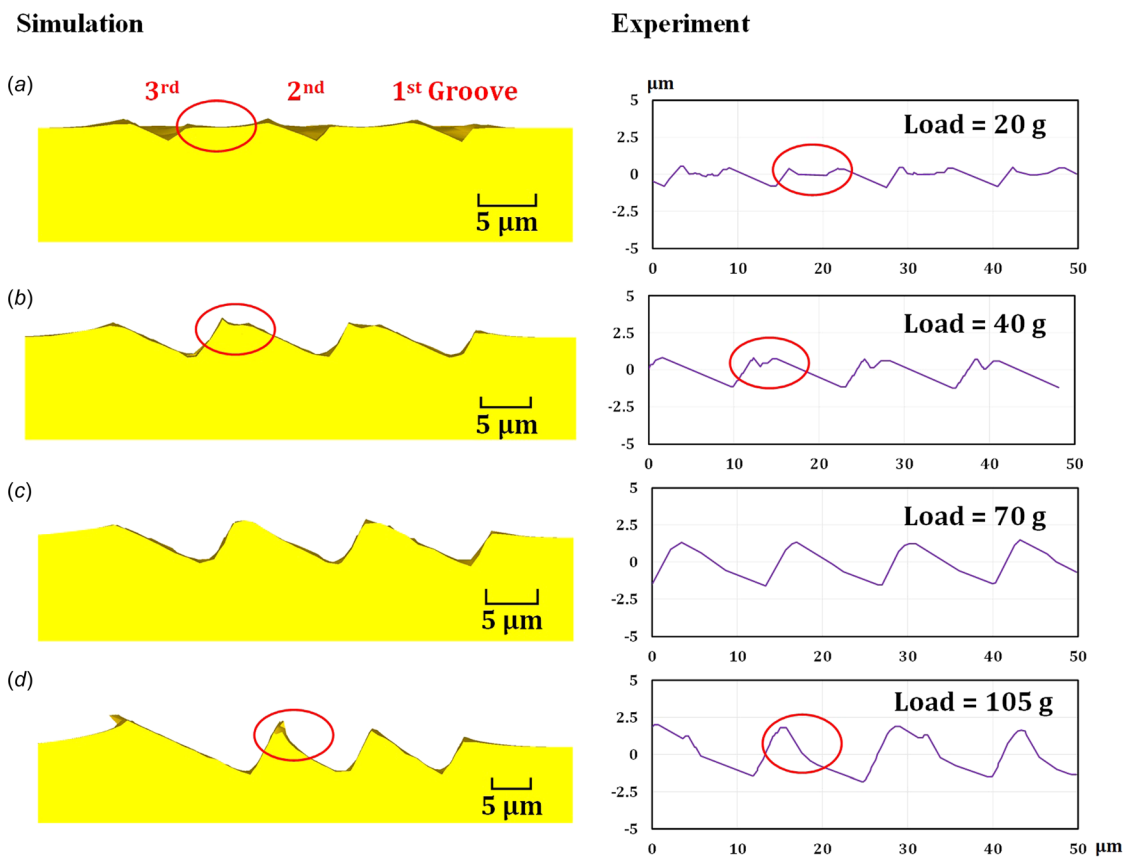

Fig. 15 Simulated and measured groove profiles under various ruling loads (with grating form defects circled): (*a*) 20 g, (*b*) 40 g, (*c*) 70 g, and (*d*) 105 g

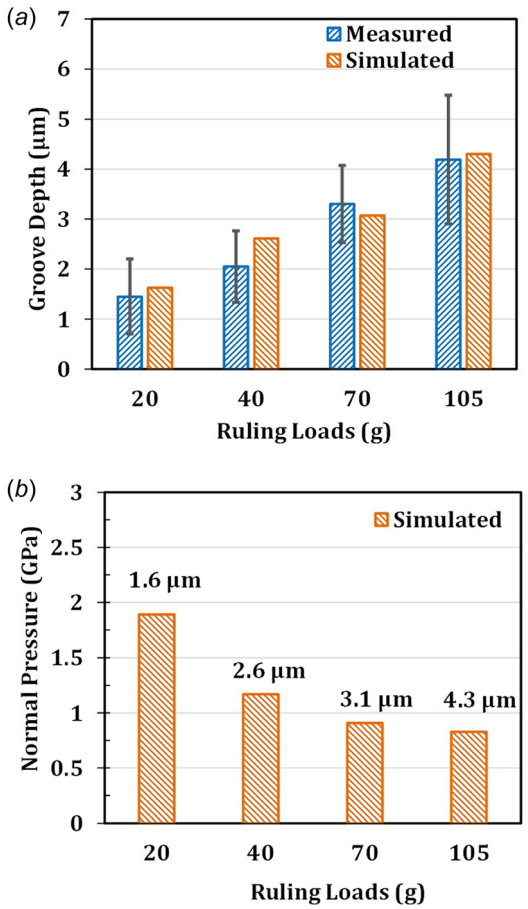

Fig. 16 Groove depth and tool normal pressure under various ruling loads: (*a*) groove depth and (*b*) tool contact pressure

groove was severely distorted by ruling of the latter groove. These simulation results demonstrated that this model has well captured the material behavior under micron-scale deformation using the strain-gradient constitutive model and accurately predict the grating groove form under various ruling loads in mechanical ruling.

Figure 16(*a*) quantitatively compares the simulated and measured groove depths from the experiments under various ruling loads. The model predicted a larger groove depth for a higher ruling load, and the predictions are close to the measured results within their measurement errors. Figure 16(*b*) shows the average contact pressure on the tool cutting surfaces predicted by the model. It was found that the tool pressure drastically decreased from 1.89 GPa at a ruling load of 20 g to 0.91 GPa and 0.83 GPa at the ruling loads of 70 g and 105 g, respectively. The significant drop in tool pressure was mostly due to the size effect of micron-scale deformation during mechanical ruling. The workpiece Al film exhibited a higher material strength for a shallow groove depth of 1.6 μm at a ruling load of 20 g than that of a groove depth of 3.1 μm at a ruling load of 70 g larger groove depth. The process temperature can also affect the normal pressure. However, due to the limited heat generation during plastic deformation and high thermal conductivity, the temperature rise was very limited as shown in Fig. 14. Therefore, the thermal effect on the tool pressure was negligible, and the size effect was considered the major factor to determine the normal pressure. These results indicated that the coupled thermomechanical analysis developed from this work can provide critical information of tool pressure under various loading conditions by considering the significant size effect of materials during the micron-scale forming process.

6 Conclusions

In this work, the material properties such as microstructure, surface morphology, and mechanical behaviors under micron-scale deformation were first characterized and experimentally analyzed using various techniques for the deposited Al film. Second, the ruled groove formation and the effect of ruling load on the form accuracy were experimentally investigated through multiple mechanical ruling experiments using a diamond tool. It was found that ruling load of 70–80 g produced the optimal grating groove geometry on the deposited Al film of 10.5 μm in thickness.

Finally, a 3D thermomechanical-coupled FE model was successfully developed to simulate the steady-state ruling pass by incorporating the nano-indentation measurement results and a strain-gradient plasticity model for predicting size effect. The groove formation with stable deformation and thermal fields was successfully simulated with a three ruling pass simulation, which agreed well with the experimental measurements. Simulation results indicated that this model has well captured the material behavior under the micron-scale groove formation and accurately predict the grating groove form under various ruling loads during the process. This model is demonstrated as a useful numerical tool for effectively designing and predicting the tool performance for mechanical ruling of various diffraction gratings.

Acknowledgment

The authors gratefully acknowledge the Changchun Institute of Optics, Fine Mechanics and Physics, Chinese Academy of Sciences for the fabrication of Al film specimens. The authors wish to gratefully acknowledge the financial support provided for the part of the study carried out at the University of Iowa by the National Science Foundation under Grant No. EPS-1101284. The authors wish to gratefully acknowledge the financial support for the nano-indentation tests provided by the Nature Science of China (Grant Nos. 51575057 and 51405031), the Nature Science of Jilin Province (Grant No. 20150101023JC), and the Science and Technology Innovation Project of Jilin Province Education Department, the College Students' Innovative Entrepreneurial Training Program (Grant Nos. 2015S015 and 2015S013).

References

[1] Carl Zeiss, 2009, "Spectral Sensors by Carl Zeiss," Oberkochen, Germany.
[2] Harrison, G. R., and Loewen, E. G., 1976, "Ruled Gratings and Wavelength Tables," Opt. Soc. Am., **15**(7), pp. 1744–1747.
[3] Harrison, G. R., and Thompson, S. W., 1970, "Large Diffraction Gratings Ruled on a Commercial Measuring Machine Controlled Interferometrically," Opt. Soc. Am., **60**(5), pp. 591–595.
[4] Carl Zeiss, 2004, "Custom Designed Gratings," Oberkochen, Germany.
[5] Wood, R. W., 1910, "Echelle Grating for the Infrared," Philos. Mag., **20**(118), pp. 770–778.
[6] Davies, D. A., and Stiff, G. M., 1969, "Diffraction Grating Ruling in Australia," Appl. Optics, **8**(7), p. 1379.
[7] Verrill, J. F., 1975, "Diffraction Grating Ruling Tool Alignment by Analysis of Traced Groove Profile," J. Phys. E: Sci. Instrum., **8**(6), pp. 522–525.
[8] Verrill, J. F., 1982, "The Effects of Diamond Wear on the Production and Properties of Ruled Diffraction Gratings Production and Properties of Ruled," J. Phys., **15**, pp. 516–519.
[9] Harada, T., Kita, T., Itou, M., Taira, H., and Mikuni, A., 1986, "Mechanically Ruled Diffraction Gratings for Synchrotron Radiation," Nucl. Instrum. Methods Phys. Res., **246**, pp. 272–277.
[10] Zhang, B., Shi, G., Shi, G., and Li, G., 2012, "Finite Element Simulation and Analysis on Wear of Mechanical Graver for Diffraction Grating," J. Theor. Appl. Inf. Technol., **46**(1), pp. 289–293.
[11] Zhang, B. Q., Shi, G. Q., and Shi, G. F., 2013, "Technical Analysis Method on Diffraction Grating Mechanical Scratching Based on Limited Elements and Cross Experiment," Key Eng. Mater., **552**, pp. 124–130.
[12] Hâkansson, G., Hultman, L., Sundgren, J.-E., Greene, J. E., and Münz, W.-D., 1991, "Microstructures of TiN Films Grown by Various Physical Vapour Deposition Techniques," Surf. Coat. Technol., **48**(1), pp. 51–67.
[13] Kadlec, S., Musil, J., and Vyskočil, J., 1992, "Growth and Properties of Hard Coatings Prepared by Physical Vapor Deposition Methods," Surf. Coat. Technol., **54–55**, pp. 287–296.
[14] Jindal, P. C., Santhanam, A. T., Schleinkofer, U., and Shuster, A. F., 1999, "Performance of PVD TiN, TiCN, and TiAlN Coated Cemented Carbide Tools in Turning," Int. J. Refract. Met. Hard Mater., **17**(1), pp. 163–170.

[15] Kim, H. J., and Joun, M. S., 2007, "Effects of Deposition Temperature and Time on the Surface Characteristics of TiN-Coated High-Speed Steel by Arc Ion Plating," J. Mech. Sci. Technol., **21**(4), pp. 575–584.
[16] Choe, H. J., Kwon, S.-H., and Lee, J.-J., 2013, "Tribological Properties and Thermal Stability of TiAlCN Coatings Deposited by ICP-Assisted Sputtering," Surf. Coat. Technol., **228**, pp. 282–285.
[17] AL-Bukhaiti, M. A., Al-hatab, K. A., Tillmann, W., Hoffmann, F., and Sprute, T., 2014, "Tribological and Mechanical Properties of Ti/TiAlN/TiAlCN Nanoscale Multilayer PVD Coatings Deposited on AISI H11 Hot Work Tool Steel," Appl. Surf. Sci., **318**, pp. 180–190.
[18] Rebelo de Figueiredo, M., Abad, M. D., Harris, A. J., Czettl, C., Mitterer, C., and Hosemann, P., 2015, "Nanoindentation of CVD Al_2O_3 Hard Coatings at Elevated Temperatures," Thin Solid Films, **578**, pp. 20–24.
[19] Oliver, C., and Pharr, M., 1992, "An Improved Technique for Determining Hardness and Elastic Modulus Using Load and Displacement Sensing Indentation Experiments," J. Mater. Res., **7**(11), pp. 1564–1583.
[20] Sokolova, E., 2004, "Simulation of Mechanically Ruled Concave Diffraction Gratings by Use of an Original Geometric Theory," Appl. Opt., **43**(1), pp. 20–28.
[21] Thornton, J. A., 1974, "Influence of Apparatus Geometry and Deposition Conditions on the Structure and Topography of Thick Sputtered Coatings," J. Vac. Sci. Technol., **11**(4), pp. 666–670.
[22] Joshi, S. S., and Melkote, S. N., 2004, "An Explanation for the Size-Effect in Machining Using Strain Gradient Plasticity," AMSE J. Manuf. Sci. Eng., **126**(4), pp. 679–684.
[23] Lai, X., Li, H., Li, C., Lin, Z., and Ni, J., 2008, "Modelling and Analysis of Micro Scale Milling Considering Size Effect, Micro Cutter Edge Radius and Minimum Chip Thickness," Int. J. Mach. Tools Manuf., **48**(1), pp. 1–14.
[24] Ding, H., Shen, N., and Shin, Y. C., 2012, "Thermal and Mechanical Modeling Analysis of Laser-Assisted Micro-Milling of Difficult-to-Machine Alloys," J. Mater. Process. Technol., **212**(3), pp. 601–613.
[25] Ding, H., and Shin, Y. C., 2013, "Multi-Physics Modeling and Simulations of Surface Microstructure Alteration in Hard Turning," J. Mater. Process. Technol., **213**(6), pp. 877–886.
[26] Ding, H., Shen, N., and Shin, Y. C., 2011, "Experimental Evaluation and Modeling Analysis of Micromilling of Hardened H13 Tool Steels," ASME J. Manuf. Sci. Eng., **133**(4), p. 041007.
[27] Gupta, N. K., Iqbal, M. A., and Sekhon, G. S., 2006, "Experimental and Numerical Studies on the Behavior of Thin Aluminum Plates Subjected to Impact by Blunt- and Hemispherical-Nosed Projectiles," Int. J. Impact Eng., **32**(12), pp. 1921–1944.
[28] Sekhon, G. S., and Chenot, J. L., 1993, "Numerical Simulation of Continuous Chip Formation During Non-Steady Orthogonal Cutting," Eng. Comput., **10**(1), pp. 31–48.
[29] Shen, N., and Ding, H., 2013, "Thermo-Mechanical Coupled Analysis of Laser-Assisted Mechanical Micromilling of Difficult-to-Machine Metal Alloys Used for Bio-Implant," Int. J. Precis. Eng. Manuf., **14**(10), pp. 1677–1685.
[30] Ding, H., and Shin, Y. C., 2012, "A Metallo-Thermomechanically Coupled Analysis of Orthogonal Cutting of AISI 1045 Steel," ASME J. Manuf. Sci. Eng., **134**(5), p. 51014.
[31] Scientific Forming Technologies Corporation, 2014, "DEFORM V11.0 (PC) Documentation," Scientific Forming Technologies Corporation, Columbus, OH.
[32] Shen, N., Samanta, A., Ding, H., and Cai, W. W., 2016, "Simulating Microstructure Evolution of Battery Tabs During Ultrasonic Welding," J. Manuf. Processes, **23**, pp. 306–314.